Neural Development

RESEARCH

Open Access

Follicle-innervating Aδ-low threshold mechanoreceptive neurons form receptive fields through homotypic competition

Matthew B. Pomaville[1,2] and Kevin M. Wright[1*]

Abstract

The mammalian somatosensory system is comprised of multiple neuronal populations that form specialized, highly organized sensory endings in the skin. The organization of somatosensory endings is essential to their functions, yet the mechanisms which regulate this organization remain unclear. Using a combination of genetic and molecular labeling approaches, we examined the development of mouse hair follicle-innervating low-threshold mechanoreceptors (LTMRs) and explored competition for innervation targets as a mechanism involved in the patterning of their receptive fields. We show that follicle innervating neurons are present in the skin at birth and that LTMR receptive fields gradually add follicle-innervating endings during the first two postnatal weeks. Using a constitutive *Bax* knockout to increase the number of neurons in adult animals, we show that two LTMR subtypes have differential responses to an increase in neuronal population size: Aδ-LTMR neurons shrink their receptive fields to accommodate the increased number of neurons innervating the skin, while C-LTMR neurons do not. Our findings suggest that competition for hair follicles to innervate plays a role in the patterning and organization of follicle-innervating LTMR neurons.

Keywords LTMR, Somatosensory neuron, Tiling, Bax, Hair follicle

Summary Statement

Aδ follicle-innervating low-threshold mechanoreceptor neurons form tiled receptive fields through competition for hair follicles during the early postnatal period.

Introduction

Mammalian somatosensation relies on the proper development, organization, and integration of multiple highly specialized sensory neuron subtypes that reside in the dorsal root ganglia (DRG) [1]. In mice, there are at least 10 identified subtypes of skin-innervating sensory neurons, which can be broadly categorized as hairy skin-innervating or glabrous skin-innervating based on their terminal ending locations [2–9]. Historically, these two groups of somatosensory neurons were subdivided based on their conduction velocity and responses to stimuli as measured by electrophysiological recordings [6, 10–12]. In hairy skin, follicles are innervated by multiple populations of low-threshold mechanoreceptive neurons (follicle-innervating LTMRs). Each LTMR neuron extends a peripherally projecting axon into the skin, where it elaborates a receptive field containing highly specialized endings around hair follicles. A series of landmark studies identified tools to genetically label somatosensory neuron subtypes, including the Aβ rapidly adapting (RA)-LTMR, Aδ-LTMR, and C-LTMR neurons, populations that were previously distinguished only by their electrophysiological characteristics [13–16]. These tools have enabled the

*Correspondence:
Kevin M. Wright
wrighke@ohsu.edu
[1] Vollum Institute, Oregon Health and Science University, Portland, OR 97239, USA
[2] Department of Cell, Developmental, and Cancer Biology, Cell and Developmental Biology Graduate Program, Oregon Health and Science University, Portland, OR 97239, USA

examination of LTMRs on a population specific and single neuron level, allowing for more detailed questions about receptive field patterning and organization mechanisms to be asked.

In adult mice, the follicle-innervating LTMR neurons form discrete and stereotyped receptive fields, innervating a constrained number of hair follicles in the skin [17]. LTMR subtypes show remarkable selectivity in the populations of hair follicles that they innervate. Aδ-LTMRs and C-LTMRs innervate both zigzag hairs and awl/auchene hairs, which comprise approximately 74% and 25% of the total hairs in the skin, respectively. Aβ RA-LTMRs form receptive fields innervating awl/auchene hairs, as well as guard hairs that comprise approximately 1% of the hairs in the skin [13, 18]. Detailed electron microscopy studies also illustrated the ultrastructure of the longitudinal lanceolate ending (LLE), its ensheathing terminal Schwann cells, and their interaction with the hair follicle [19]. These studies together laid the groundwork for molecularly driven exploration into the development and function of follicle-innervating neurons.

The strict organization of follicle innervating neurons into constrained receptive fields is essential for the proper localization of touch stimulus on the body. Recently, advancements in genetically driven multi-fluorophore reporter systems made it possible to examine the interactions between neurons of the same genetic subtype in adult mice. These studies showed that Aδ-LTMR and C-LTMR neurons form tiled receptive fields with minimal overlap between neighboring homotypic neurons. In contrast, Aβ RA-LTMR neurons form receptive fields that overlap with those of neighboring Aβ RA-LTMR neurons, resulting in LLEs from multiple Aβ RA-LTMR neurons at each guard hair [18]. The mechanisms by which follicle-innervating LTMR neurons form exclusive receptive fields remains largely unexplored.

The homotypically tiled arrangement of Aδ-LTMRs and C-LTMRs in mice is reminiscent of the innervation patterns of dendritic arborization (DA) neurons in larval *Drosophila melanogaster* epidermis [20]. The four DA neuronal subtypes show differing capacities for homotypic receptive field arrangement. Class IV and III DA neurons tile the body wall with differing degrees of receptive field overlap, while Class I and II DA neurons show no repulsive response to homotypic neurons [21]. Tiled dendritic receptive fields have also been observed in neurons innervating the epidermis in *Manduca sexta* and *Haementeria ghilanii* [22–24]. The paradigm of sensory neuron receptive field patterning is also present in vertebrate systems. *Danio rerio* trigeminal neurons arrange at the midline through repulsive mechanisms like those seen in *Drosophila* [25]. In the mouse retina, multiple examples of dendritic tiling and population-based organization exist. Bipolar cell subtypes and horizontal cells tile to innervate all available photoreceptor terminals while excluding neighboring homotypic dendritic fields and can adjust their receptive field size to accommodate changes in population [26, 27]. In contrast, some amacrine cells show substantial overlap of dendritic arbors with homotypic neighbors and maintain dendritic field size even when cell density is altered [28–30].

In this study, we closely examine the development and maturation of hair follicles and follicle-innervating LTMR neurons over the first three postnatal weeks in mice. We test the hypothesis that LTMRs tile their receptive fields through a process which responds to increases in neuronal population by generating smaller receptive fields. We show that follicle innervation and hair follicle maturation coincide during the early postnatal window (before postnatal day 7, P7), and that by P14, follicle-innervating LTMR receptive fields have similar numbers of mature LLEs as adult receptive fields. Finally, using genetic tools to sparsely label single follicle-innervating LTMR neurons, we show that Aδ-LTMR form receptive fields through homotypic competition during the early postnatal period.

Results

Mouse hair follicle maturation occurs during the early postnatal window

Follicle-innervating LTMR neurons are highly branched in the skin to form receptive fields of highly specialized LLEs around hair follicles. Each follicle-innervating LTMR subtype selectively innervates specific hair follicle subtypes (Fig. 1A). However, the process by which this occurs during development is poorly understood. To understand the temporal relationship between hair follicles and LTMRs during development, we first characterized the postnatal maturation of hair follicles. Previous literature characterizing hair follicle maturation demonstrated that hair follicles are established in multiple waves starting at embryonic day 15 (E15) and continue through P9, when all hair follicles have a mature structure, including a hair shaft emerging from the skin [31]. To assess hair follicle density during the early postnatal period, back skin was collected from mice at time points between P0 and P60 (Fig. 1B-G). Hair follicles could be easily identified as cell-dense structures in skin sections by staining with the nuclear marker DAPI. Hair follicle density was calculated by counting the number of hair follicle structures (long DAPI-dense structures) present in a known length of skin. Hair follicle density initially remains stable from P1-P6, then decreases beginning at P14 as mice grow more rapidly (Fig. 1H, Supplementary Table 1). This decrease in density corresponds with hair follicles completing their passage through the hair follicle

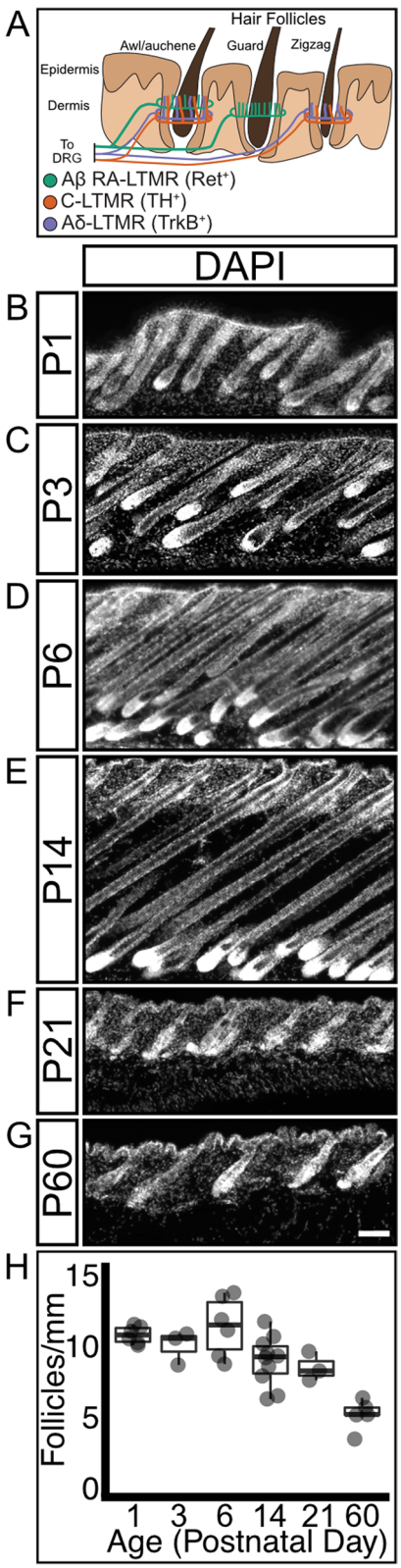

Fig. 1 Mouse hair follicle density decreases as mice age. **A** Schematic showing hair follicle-innervating LTMR neuron subtypes projecting to the skin, where their axons branch and selectively innervate specific hair follicle types. **B**-**G** Sagittal sections of mouse back skin stained with DAPI to highlight hair follicle structures. Section height increases, then decreases as mice age and progress through the hair follicle life cycle. Scale bar – 50 µm. **H** Hair follicle density remains stable for the first week of postnatal life, then decreases as mice grow. *N* = 6(P1), 3(P3), 6(P6), 10(P14), 3(P21), 5(P60)

cycle, as can be seen by the changes in dermal thickness over time [32].

We further analyzed the changes in hair follicle density by normalizing the density measurements for each timepoint to the average body length of a cohort of age-matched mice (Fig. S1A). This normalization supports the conclusion that hair follicle density decreases as mice grow, and that the density of hair follicles decreases more than would be expected if mice were adding hair follicles at a rate that kept pace with animal growth (Fig. S1B). From these data, we conclude that hair follicle maturation occurs rapidly in the early postnatal window and that the rate of hair follicle addition decreases in maturing mice.

Sensory neurons form specialized endings concurrently with hair follicle maturation

We next examined the developmental time course of hair follicle innervation using the pan-neuronal marker β-III Tubulin. We quantified the proportion of hair follicles with a β-III Tubulin-positive nerve ending encircling the follicle at multiple developmental timepoints from P1-P60 (Fig. 2A-F). Axons are present in the dermis and epidermis at P1, but very few innervate hair follicles at this age (Fig. 2A, G). While axon branches are present at the expected depth for follicle-innervating LLEs (inset region, Fig. 2A) , these neurite branches do not yet encircle the hair follicle. There is a significant increase in the proportion of innervated hair follicles at P3, with over half of hair follicles encircled by a β-III Tubulin-positive axon (Fig. 2B, G). At P3 the encircling endings have not formed the LLE projections characteristic of follicle-innervating LTMRs. By P6 the innervation of hair follicles is nearly complete and the characteristic LLEs have appeared, projecting towards the epidermal surface along the hair shaft from the encircling neurite (Fig. 2C and inset, 2G). By P14, hair follicle innervation is complete, and the proportion of innervated hair follicles and LLE morphology remains unchanged at P21 and P60 (Fig. 2D-F, G, Supplementary Table 1). These findings are largely in agreement with other studies and suggest

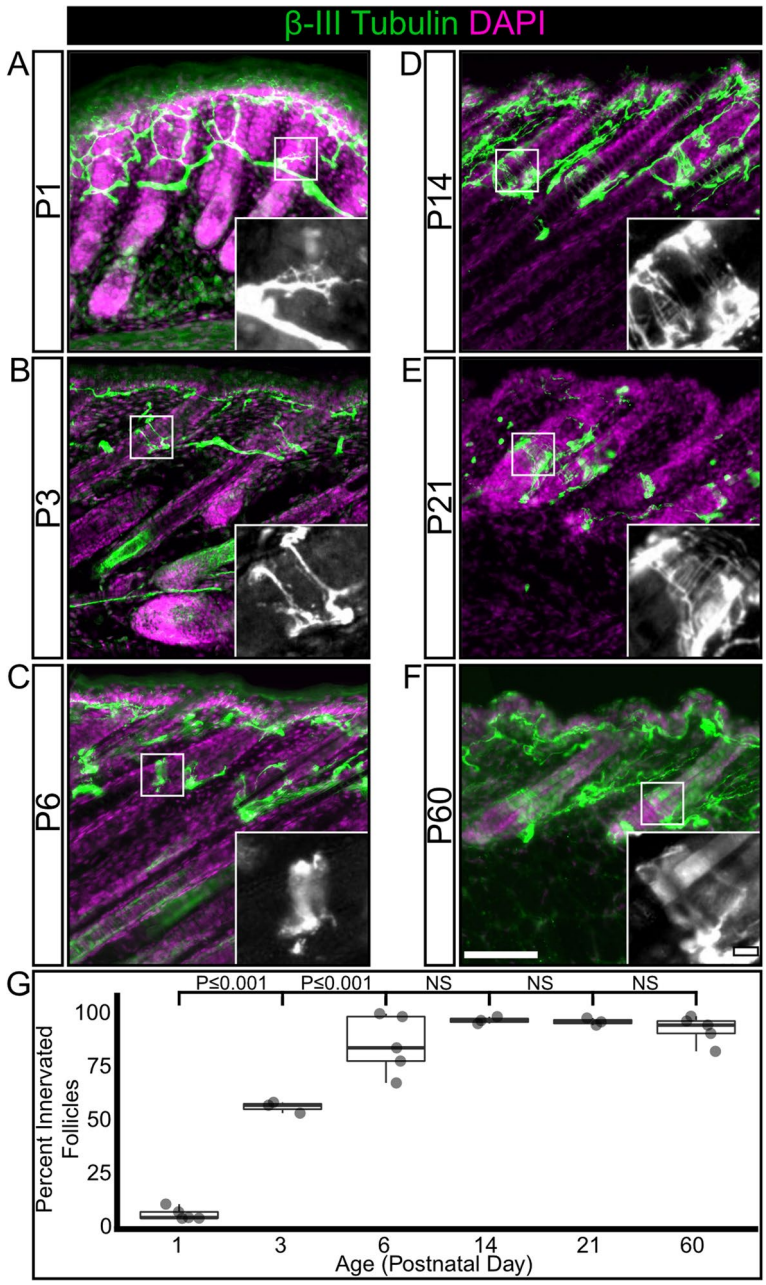

Fig. 2 The percentage of innervated hair follicles increases during the first postnatal week, then remains stable into adulthood. **A**-**F** Representative images of hair follicle innervation labeled with a pan-neuronal marker (β-III Tubulin, green) and DAPI (magenta). Mature longitudinal-lanceolate endings begin to appear by P6. Insets – Single channel images of follicle innervation. Scale bar – 50 μm, insets – 10 μm. **G** Quantification of the percentage of hair follicles innervated by a β-III Tubulin positive axon. One-way ANOVA with Tukey's HSD post-hoc testing (ANOVA $P \leq 0.001$, P1-P3 $P \leq 0.001$, P3-P6 $P \leq 0.001$) $N = 5$(P1), 3(P3), 5(P6), 3(P14), 3(P21), 5(P60)

that murine hair follicle innervation occurs during the early postnatal window, and that by the end of the first postnatal week hair follicle innervation has reached a grossly mature state [33, 34].

Aβ RA-LTMR follicle innervation precedes C-LTMR and Aδ-LTMR follicle innervation

We next investigated whether there is a temporal hierarchy of hair follicle innervation between LTMR subtypes.

To assess the development of hair follicle innervation by specific LTMR subtypes, we utilized three separate labeling strategies. Based on data from single-cell RNA sequencing performed on adult dorsal root ganglia neurons and previous studies examining LTMR development, we identified ubiquitous markers for Aβ RA-LTMRs (anti-Calbindin immunohistochemistry) and C-LTMRs (*Vglut3*^{iCre} driven *TdTomato* expression (*Ai9*)), and an inducible marker for Aδ-LTMRs (*TrkB*^{CreERT2} driven placental alkaline phosphatase (*R26*^{iAP}) reporter) [16, 35–39].

Calbindin^{+} Aβ RA-LTMRs innervate guard (tylotrich) hairs, which make up approximately 1% of the hair follicles in mouse skin, and awl/auchene hairs which make up approximately 25% of the follicles [18, 19]. At P1, there are very few Calbindin^{+} follicle-encircling nerve endings present (Fig. 3A, G), but by P3 the proportion of hair follicles with Calbindin^{+} encircling LTMR endings has significantly increased to approximately adult levels (Fig. 3B, G) and remains stable through at least P60 (Fig. 3C-F, G, Supplementary Table 1). C-LTMRs innervate the two families of non-tylotrich hairs, the zigzag hairs (~74% of hair follicles) and the awl/auchene hairs [18, 19]. At P1, Vglut3^{+} C-LTMR axons are present in the skin but there are few follicle-innervating nerve endings present (Fig. 3H, N). The proportion of C-LTMR-innervated hair follicles significantly increases between P1 and P3, with over half of hair follicles receiving innervation from a C-LTMR axon ending (Fig. 3I, N). By P6 the proportion of C-LTMR innervated hair follicles has increased to approximately adult levels, where it remains stable (Fig. 3J-M, N, Supplementary Table 1).

To explore the timing of Aδ-LTMR receptive field development, we crossed the inducible *TrkB*^{CreERT2} line with a *Cre*-inducible GFP reporter line (*Ai140D*) to sparsely label Aδ-LTMRs, and imaged receptive fields at multiple time points [16, 40, 41]. The Aδ-LTMRs were ideal for developmental receptive field analysis as they were genetically accessible with prenatal tamoxifen administration and *TrkB*^{CreERT2} labels a stable population of cells throughout development. In the first 24 h after birth, there are few follicle-innervating nerve endings present in the skin, though TrkB^{+} Aδ-LTMR axons are present and have begun to branch (Fig. 4A, E). At P3 the neurons have begun to form follicle-innervating endings (Fig. 4B, arrowheads, 4E), but still contain many non-follicle-innervating neurites (Fig. 4B, E). The transition from non-ending forming neurites to follicle-innervating endings continues at P6 (Fig. 4C, E). By P14 the receptive fields resemble those in mature animals, with few non-follicle-innervating neurites present, and hemicircular LLEs are present at most hair follicles in the innervated area (Fig. 4D, E, Supplementary Table 2). The completion of Aδ-LTMR development is further confirmed in sections of P14 skin co-labeled with β-III Tubulin and *TrkB*^{CreERT2};*R26*^{iAP} driven with multiple high prenatal doses of tamoxifen (Fig. S2A-C). Quantification of the proportion of hair follicles innervated by a TrkB^{+}/β-III Tubulin $^{+}$ ending shows innervation matching expected proportions in adult animals (92.2% ± 3% s.e.m.). Taken together, these data show that innervation of hair follicles by LTMRs is an ongoing process during the first two postnatal weeks, and there is a subtype-specific temporal hierarchy of hair follicle innervation, with Calbindin^{+} Aβ RA-LTMRs preceding both Vglut3^{+} C-LTMRs and TrkB^{+} Aδ-LTMRs.

Competition between Aδ-LTMRs shapes their receptive fields

Many sensory neurons tile their receptive fields in order to reduce homotypic overlap [20–22, 25]. Of the hair follicles innervated by C-LTMRs, < 30% are innervated by multiple C-LTMRs; for Aδ-LTMRs, < 10% are innervated by multiple Aδ-LTMRs [18]. We hypothesized that this near-exclusive pattern of receptive field innervation is the result of homotypic competition for territory. If this were true, we would expect individual neurons of a given subtype to adjust their receptive field size in response to changes in neuronal subtype population. We developed a genetic strategy to test this hypothesis using deletion of the proapoptotic protein *Bax* to generate a model of neuronal overpopulation. Deletion of *Bax* blocks developmental programmed cell death in DRG neurons and results in 50–70% increases in the number of TrkA, TrkC, TrpV1, and CGRP-positive DRG neurons [42–44]. However, the effect of *Bax* deletion on LTMR populations has not previously been assessed.

To quantify the effect of *Bax* deletion on Aδ-LTMR and C-LTMR populations, we collected cryosections from the sixth thoracic DRG, which contains the neurons responsible for innervating the thoracic skin but contains no limb or glabrous skin innervating neurons [45]. Sections were labeled with markers for sensory neurons (Islet 1/2, Fig. 5A, D), C-LTMRs (Tyrosine Hydroxylase (TH), Fig. 5B, E), and Aδ-LTMRs (*TrkB*^{CreERT2}; *R26*^{iAP}, (see methods) Fig. 5C, F), and the number of marker-positive cell bodies in the imaged sections was manually counted. Cell counts from wild-type and heterozygous mice showed no significant differences in any comparison (Fig. S3A-C). All knockout neuron counts were normalized to control heterozygous littermates to account for litter-to-litter variation arising from tamoxifen administration and alkaline phosphatase staining. We found an overall 20% increase in the number of Islet 1/2-positive neurons in *Bax*$^{-/-}$ animals compared to control animals.

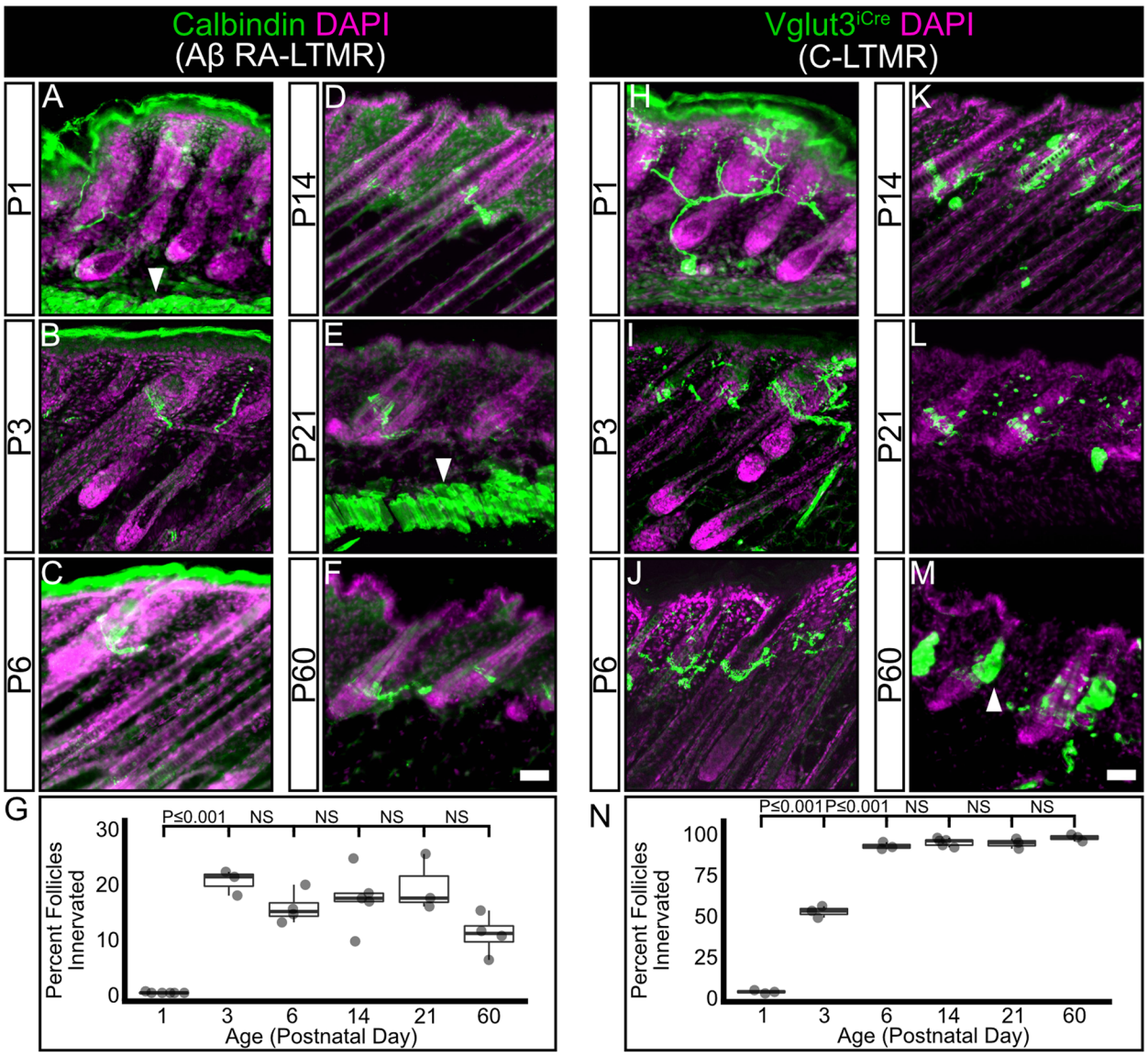

Fig. 3 Aβ RA-LTMR neurons complete innervation of hair follicles before C-LTMR neurons. **A**-**F** Representative images of hair follicle innervation labeled with a Aβ RA-LTMR specific marker (Calbindin, green) and DAPI (magenta). Mature longitudinal-lanceolate endings begin to appear by P3. Arrowheads (A, E) – Subcutaneous muscle autofluorescence, Scale bar – 50 µm. **G** Quantification of the percentage of hair follicles innervated by a Calbindin positive Aβ RA-LTMR axon. The percentage of innervated hair follicles reaches its maximum level by P3. One-way ANOVA with Tukey's HSD post-hoc testing (ANOVA $P \leq 0.001$, P1-P3 $P \leq 0.001$). $N = 6$(P1), 3(P3), 4(P6), 5(P14), 3(P21), 4(P60). **H**-**M**) Representative images of hair follicles innervated by Vglut3 + axons (*Vglut3*^{iCre}*;TdTomato*, green) and DAPI (magenta). Mature longitudinal-lanceolate endings begin to appear by P3. Arrowhead (M) – Sebaceous gland autofluorescence, Scale bar – 50 µm. **N** Quantification of the percentage of hair follicles innervated by a *Vglut3*.^{iCre}*;TdTomato* positive C-LTMR axon. The percentage of innervated hair follicles increases between P1 and P3, and reaches its maximum level by P6. One-way ANOVA with Tukey's HSD post-hoc testing (ANOVA $P \leq 0.001$, P1-P3 $P \leq 0.001$, P3-P6 $P \leq 0.001$). $N = 3$(P1), 3(P3), 3(P6), 5(P14), 3(P21), 3(P60)

The number of *TrkB*$^{CreERT2+}$ Aδ-LTMRs showed a significant increase (33%) in *Bax*$^{-/-}$ animals compared to control littermates. The number of TH^{+} C-LTMRs increased 24% in *Bax*$^{-/-}$ animals compared to control littermates, which was not statistically significant due to variation in cell numbers (Fig. 5G, Supplementary Table 3). Deletion of *Bax* had no effect on hair follicle density in P21 mice, as measured using Oil Red O staining (Fig. S4A-D). Therefore, *Bax* deletion results in a significant overpopulation of Aδ-LTMR neurons but does not significantly affect the number of

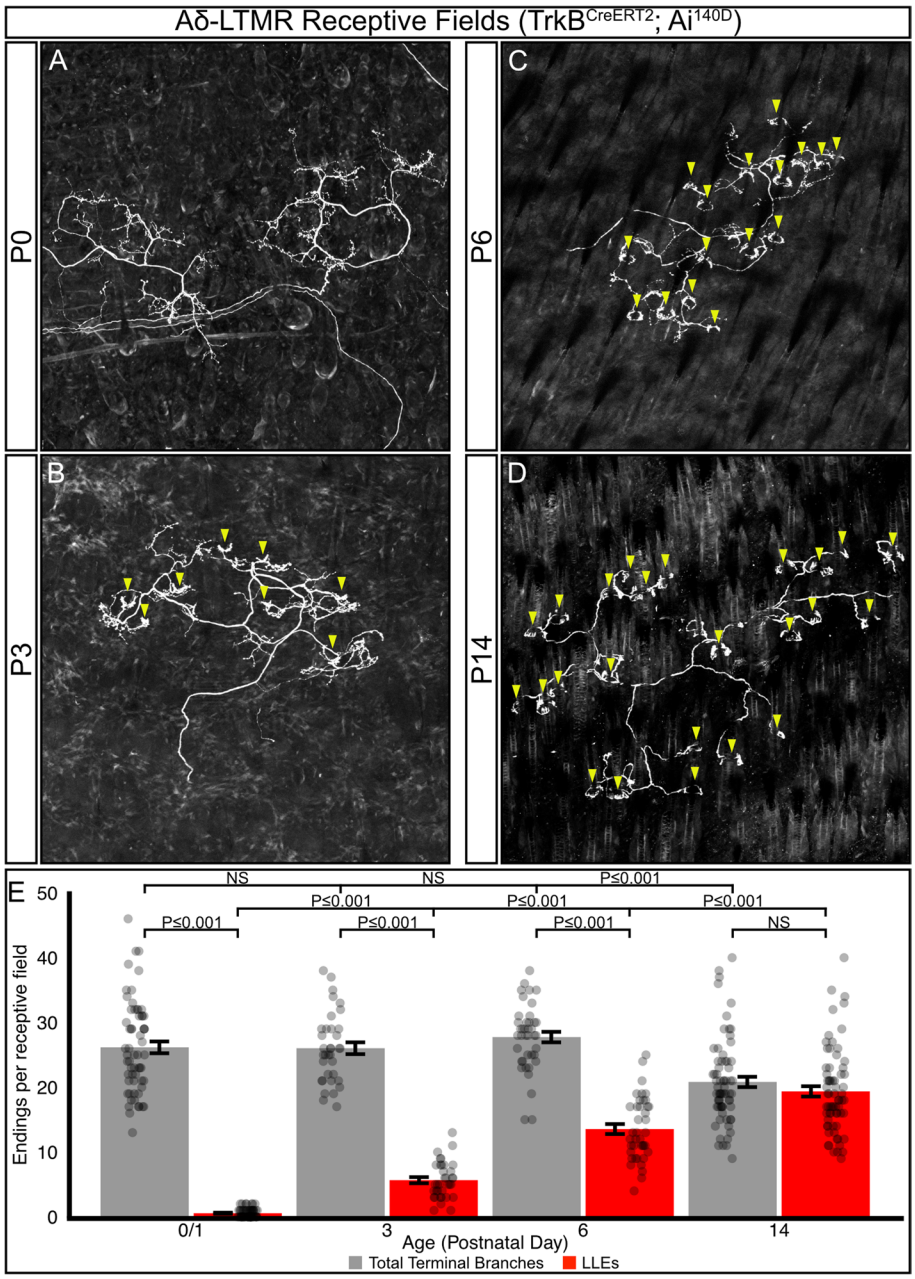

Fig. 4 Aδ-LTMRs develop longitudinal-lanceolate endings (LLEs) after elaboration/branching in the first postnatal week. **A**-**D** Representative images of sparsely labeled Aδ-LTMR receptive fields in mouse back skin. Aδ-LTMR axons are present in the skin at P0 (A, two distinct adjacent RFs shown). Follicle-innervating LLEs first appear by P3 (**B**); more follicle-innervating endings are present in P6 animals (**C**), and by P14 nearly all terminal branches end in LLEs (**D**). Arrowheads – Follicle-innervating LLEs. Scale bar – 100 µm. **E** Quantification of the number of terminal branches per receptive field (grey) and the number of terminal LLEs per receptive field (red). Points represent individual receptive fields. Bars represent mean ± s.e.m. Total number of receptive fields quantified and (number of animals): P0/1: 61(4), P3: 35(3), P6: 40(3), P14: 68(3) Total branches: ANOVA $P \leq 0.001$, LLEs: ANOVA $P \leq 0.001$, Total branches vs LLEs: P0/1 Wilcoxon Rank Sum Test $P \leq 0.001$, P3 Wilcoxon Rank Sum Test $P \leq 0.001$, P6 Wilcoxon Rank Sum Test $P \leq 0.001$, P14 Wilcoxon Rank Sum Test $P \geq 0.05$

C-LTMR neurons or the targets of LTMR innervation (hair follicles).

If LTMRs of the same subtype compete for territory, we would expect that the receptive fields of individual Aδ-LTMRs would become smaller in *Bax*$^{-/-}$ animals to accommodate the excess number of neurons, while the receptive fields of C-LTMRs would remain largely unchanged. To test this, we generated triple transgenic

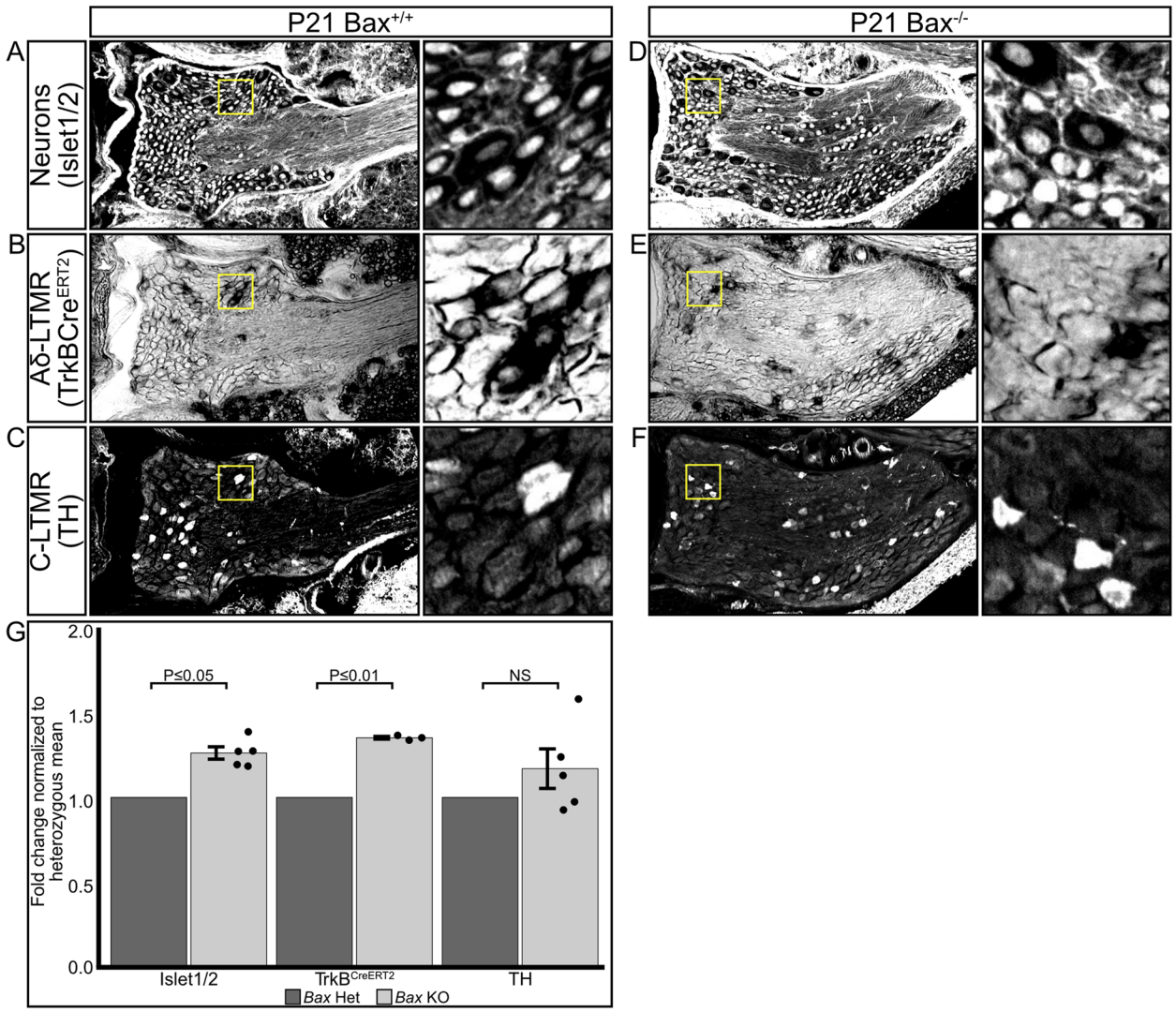

Fig. 5 Genetic deletion of the proapoptotic protein *Bax* has differential effects on LTMR populations. **A**-**F**) Representative sections of T6 dorsal root ganglia from 21-day old wild-type littermates (**A**-**C**) and *Bax* knockout (**D**-**F**) mice labeled with markers for neuronal nuclei (A, D Islet 1/2), Aδ-LTMR cell bodies (B, E TrkB^{CreERT2}; R26^{iAP}), C-LTMR cell bodies (C, F Tyrosine Hydroxylase). Scale bar – 50 µm. Insets show high-magnification of boxed regions. **G** Quantification of the change in T6 DRG LTMR neuron proportions in *Bax* knockout animals normalized to the mean number of heterozygous littermates. Bars represent mean ± s.e.m. *N* = Islet 1/2: Het – 7, KO – 5, TrkB: Het – 5, KO – 3, TH: Het – 7, KO – 5. Islet 1/2 Wilcoxon Rank Sum: $P \leq 0.040$, TrkB.^{CreERT2} Wilcoxon Rank Sum: $P \leq 0.007$, TH Wilcoxon Rank Sum: $P > 0.089$

mice carrying 1: tamoxifen inducible *Cre* driver lines for Aδ-LTMRs (*TrkB*^{CreERT2}) or C-LTMRs (*TH*$^{IRES-CreER}$), 2: a *Cre*-dependent placental alkaline phosphatase reporter (*R26*^{iAP}), and 3: *Bax*$^{+/+}$, *Bax*$^{\pm}$, or *Bax*$^{-/-}$ [16, 46–48]. We administered low doses of tamoxifen to timed-pregnant dams (Aδ-LTMRs) or juvenile mice (C-LTMRs) to sparsely label receptive fields and quantified the number of hair follicles in each receptive field of young adult animals (P21). Representative images of Aδ-LTMR and C-LTMR receptive fields (Fig. 6A-G) from *Bax*$^{+/+}$, *Bax*$^{\pm}$, and *Bax*$^{-/-}$ mice were traced using the FIJI plugin Simple Neurite Tracer (Fig. 6A-G) to better illustrate the receptive field structure [49, 50]. Aδ-LTMRs showed a significant reduction in the number of hair follicles innervated by each neuron in *Bax*$^{-/-}$ animals (24.2 ± 0.5 s.e.m. follicles/neuron) compared with both wild-type (31.6 ± 0.8 s.e.m. follicles/neuron) and heterozygous (29.5 ± 0.5 s.e.m. follicles/neuron) animals (Fig. 6D). This represents a 23% decrease in the number of hair follicles innervated by single Aδ-LTMRs in *Bax*$^{-/-}$ animals. In contrast to the Aδ-LTMRs, there was no significant difference in the number of hair follicles innervated by each

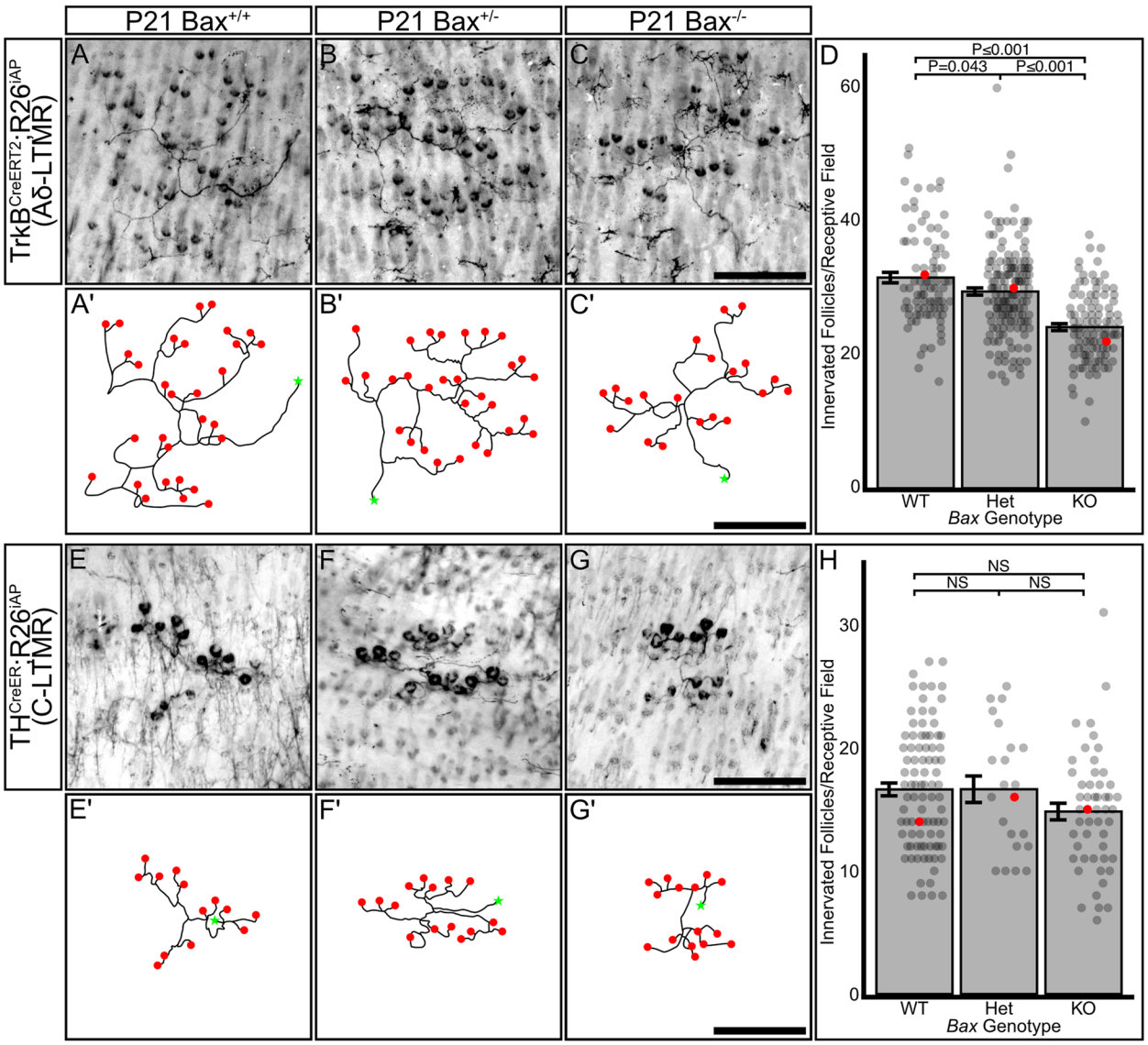

Fig. 6 Aδ-LTMRs adjust their receptive field size to accommodate changes in neuronal population due to *Bax* deletion. **A**-**C**') Representative images and traced reconstructions of isolated Aδ-LTMR receptive fields from back skin of P21 *TrkB*^{CreERT2}; *R26*^{iAP}; *Bax* wild-type (A, A'), heterozygous (B, B'), and knockout (C, C') animals. Red dots in traces correspond with hair follicles, green stars indicate the axon segment from which the traced RF originates. Scale bar – 250 µm. **D** Quantification of the number of hair follicles innervated by each Aδ-LTMR receptive field in *TrkB*^{CreERT2};*R26*^{iAP}; *Bax* wild-type, heterozygous, and knockout animals. Receptive fields in *Bax* knockout animals innervate fewer hair follicles than wild-type and heterozygous animals. Each dot represents one receptive field, red dots represent the data point from to the associated representative image. Bars represent mean ± s.e.m. One-way AONVA with Tukey's HSD post-hoc testing ANOVA $P \leq 0.001$, WT-KO $P \leq 0.001$, Het-KO $P \leq 0.001$, WT-Het $P = 0.043$. Number of individual receptive fields (number of animals): WT: 85(3), Het: 154(5), KO: 103(3). **E**–**G**' Representative images and traced reconstructions of isolated C-LTMR receptive fields from back skin of P21 *TH*^{CreERT2}; *R26*^{iAP};*Bax* wild-type (E, E'), heterozygous (F, F'), and knockout (G, G') animals. Red dots in traces correspond with hair follicles, green stars indicate the axon segment from which the traced RF originates. Scale bar – 250 µm. **H** Quantification of the number of hair follicles innervated by each C-LTMR receptive field in *TH*^{CreERT2}; *R26.*^{iAP};*Bax* wild-type, heterozygous, and knockout animals. No significant difference was seen in the number of hair follicles innervated across *Bax* genotypes. Each dot represents one receptive field, the red dots represent the data point from to the associated representative image. Bars represent mean ± s.e.m. One-way AONVA, $P = 0.098$. Number of individual receptive fields (number of animals): WT: 90(6), Het: 22(4), KO: 51(3)

C-LTMR receptive field in *Bax*$^{-/-}$ (14.8 ± 0.7 s.e.m. follicles/neuron), heterozygous (16.6 ± 1.1 s.e.m. follicles/neuron), or wild-type (16.6 ± 0.5 s.e.m. follicles/neuron) animals (Fig. 6H). No significant differences were seen between mice of the same *Bax* genotype across litters for both Aδ-LTMRs and C-LTMRs (Fig. S5A-B). Therefore, we conclude that follicle-innervating Aδ-LTMR form their receptive fields through homotypic competition.

Discussion

The organized development of skin- and hair follicle-innervating sensory neurons is essential for communicating meaningful information about touch to the brain in order to moderate behavior. In this study we make use of multiple cell-type specific molecular and genetic tools to analyze the development of hair follicle innervation and explore the principles that govern follicle-innervating LTMR receptive field organization. We show innervation of hair follicles and initial LLE development occurs during the first two postnatal weeks, and that by P14, mice show an adult innervation pattern. We also show that LTMR subtypes have a differential dependence on Bax-mediated developmental apoptosis, with Aδ-LTMRs responding to deletion of *Bax* by significantly increasing their population, while the population of C-LTMRs increases only slightly. Finally, we demonstrate that in response to this change in population, Aδ-LTMR neurons shrink their receptive fields to accommodate their neighbors.

LTMR receptive fields undergo gradual refinement during the first two postnatal weeks

Previous work has described the tight association between hair follicles and the follicle-innervating LTMRs, showing PGP9.5 labeled axons wrapping hair follicles as early as E18, and describing the adult morphology of LTMRs in a population-specific manner [13, 16, 17, 19, 33]. Our work builds upon this by analyzing the development of follicle innervation during the first three postnatal weeks in an LTMR-subtype-specific manner. Specifically, we present a detailed timeline showing a gradual development of follicle innervation by Aβ RA-LTMRs and C-LTMRs during the first two postnatal weeks (Fig. 3). We also used a genetically-driven sparse labeling approach to examine the development of individual Aδ-LTMR receptive fields, showing a gradual development of follicle-innervating endings and refinement of LTMR receptive field characteristics during the first two postnatal weeks (Fig. 4). These findings agree with recent work describing interactions between LTMR axons and terminal Schwann cells at the hair follicle during this time period [34].

Follicle innervation develops in a temporally ordered manner

Our detailed examination of LTMR follicle innervation development revealed a temporal hierarchy for the different subtypes, with Aβ RA-LTMRs completing their innervation of hair follicles by P3, before C-LTMRs and Aδ-LTMRs do at P6 (Fig. 3). Recent comparison of the development of Aβ RA-LTMRs and Aδ-LTMRs supports this conclusion, showing Aβ RA-LTMRs maturing at P3 and Aδ-LTMRs maturing after P6 [34]. This temporal hierarchy parallels the maturation of hair follicle subtypes. Guard hair placodes, which are innervated by Aβ RA-LTMRs, consolidate between E14 and E15, with the first guard hair shafts appearing between E16 and E18. The consolidation of other hair follicle placodes, which are innervated by C-LTMRs and Aδ-LTMRs, occurs in successive waves continuing until after birth [33, 51, 52]. This temporal hierarchy of innervation could also be due to the temporal order of LTMR differentiation. EdU birth dating studies have shown that Aβ RA-LTMR neurons are born as early as E9.5 and have a peak birth rate at E10.5 before sharply dropping off. In contrast, C-LTMRs and Aδ-LTMRs are born approximately one day later, peaking at E11.5 and gradually tapering off by E13.5 [53]. Furthermore, single-cell transcriptomic analysis of the developing DRG shows that C-LTMRs are among the last populations to mature as transcriptionally distinct subtypes, mirroring their birthdate hierarchy [39]. It is tempting to speculate that early-born Aβ RA-LTMRs could be a "pioneer" axon population in the periphery, functioning as a scaffold along which axons from Aδ-LTMRs and C-LTMRs grow before branching to form receptive fields. In invertebrate systems, pioneer axons play a critical role in establishing peripheral innervation patterns, and ablation of these cells leads to significant disruptions in follower axons [54–58]. In vertebrates, early extending axons often act as a permissive substrate upon which later-born neurons can extend their axons, but the necessity of these early-extending axons is less clear [59–61]. In an interesting parallel, Ret is expressed in both early-born Aβ RA-LTMRs and in a population of pioneer axons in the zebrafish posterior lateral line [62]. Future studies will be required to determine if early born Ret^+ Aβ RA-LTMRs function as pioneers in the mouse DRG.

Knockout of the proapoptotic protein *Bax* shows differential effects on LTMR populations

To understand how competition between LTMR neurons might influence receptive field development, we devised a genetic strategy to drive LTMR overpopulation by blocking developmental apoptosis. Multiple studies have demonstrated that sensory neurons are initially overproduced, followed by a wave of developmental apoptosis regulated by target-derived factors which ensures neurons and targets are appropriately matched [Reviewed in [63–65]. Genetic deletion of the pro-apoptotic protein *Bax* blocks developmental apoptosis and results in significantly increased numbers of neurons in the DRG [66, 67]. While *Bax* knockout animals show a 1.5-fold to 1.8-fold increase in the population of proprioceptive and

nociceptive DRG neurons and increased sensory axon density in the paw, previous studies had not examined the effect of *Bax* deletion on populations of LTMRs [42]. Our experiments specifically examining follicle-innervating LTMRs showed a significant increase in the number of Aδ-LTMR (*TrkB*$^{+}$) DRG neurons, but not in C-LTMR (*TH*$^{+}$) DRG neurons. These results reveal an interesting difference in the dependence of different neuronal LTMR subtypes on developmental apoptosis to achieve their final numbers. The basis for this difference is unknown, but may involve mechanisms related to the specification, differentiation, and/or organization of LTMR neurons, such as the role for target-derived trophic cues in LTMR population determination and LLE maintenance.

Homotypic competition plays a role in LTMR receptive field organization

The development of tools for subtype-specific labeling of LTMRs revealed several interesting organizational properties. First, different LTMR subtypes have different hair follicle innervation patterns, with Aβ RA-LTMRs innervating guard and awl/auchene hairs, while Aδ-LTMRs and C-LTMRs innervate zigzag and awl/auchene hairs. Second, LTMRs have distinct, highly stereotyped receptive fields that typically innervate a fixed range of hair follicles [13, 16, 17, 19]. In our study, we attempted to address these properties at a cellular level by examining the role of homotypic competition in the establishment of receptive fields. We reasoned that inducing overpopulation of LTMR subtypes with *Bax* deletion would lead to two potential outcomes. Either neurons would decrease their receptive field size to accommodate the increased number of neighbors and preserve homotypic tiling, or they would maintain their receptive field size at the expense of tiling. Aδ-LTMRs showed a clear preference for adjusting their receptive field size to accommodate the population increase, with each neuron in *Bax*$^{-/-}$ mice forming a receptive field innervating significantly fewer hair follicles than in wild-type mice. In contrast, the number of C-LTMRs in *Bax* deficient mice was not significantly different from controls, and these neurons did not adjust their receptive field size. This difference could be due to the stringency of the tiling behaviors of the two LTMR subtypes: approximately 10% of hair follicles in wild-type mice are innervated by two distinct Aδ-LTMRs, whereas 25% of hair follicles are innervated by two distinct C-LTMRs [18]. We attempted a complementary approach, ablating a portion of the Aδ-LTMR population prenatally using the *TrkB*^{CreERT2} driver crossed to a *Cre*-dependent sensory neuron specific Diphtheria toxin receptor (*Avil*^{iDTR}), reasoning that population depletion before follicle innervation would result in larger receptive fields [68]. Unfortunately, these experiments resulted in perinatal lethality, potentially due to off-target effects of Diphtheria toxin administration.

At the molecular level, there is little known about the cues that regulate the targeting of LTMR subtypes to specific hair follicle types or the establishment of receptive fields. While BDNF derived from hair follicle-associated epithelial cells is important for the polarized innervation pattern and LLE maturation of TrkB^{+} Aδ-LTMR axonal endings, it is dispensable for the initial attraction of Aδ-LTMR axons to hair follicles, and it is unknown whether it regulates receptive field size [16]. Similarly, recent work has shown that the GPI-linked receptor Netrin-G1 is required in LTMRs for the proper maturation of terminal endings around hair follicles, but not for terminal axon branching or receptive field size [34]. In contrast, ɣ-Protocadherins are important for the peripheral branching and innervation of non-guard hair follicles by Aβ-LTMRs, but not for the maturation of LLEs [6, 69]. Together, these data suggest that the initial innervation of hair follicles and the morphological maturation of their terminal endings are distinct events regulated by different molecular pathways. Interestingly, terminal Schwann cells are the source for ligands/binding partners for both Netrin-G1 and ɣ-Protocadherins in LTMRs, demonstrating that they play a critical role in regulating hair follicle innervation [34, 69].

Why do distinct LTMR subtypes display different receptive field morphologies? Presumably, tight regulation of LTMR receptive field size and organization is intrinsically tied to their sensory functions. In order to allow for precise localization of a stimulus, cutaneous sensory neurons must innervate a constrained area of the skin and relay this information to the proper regions of the central nervous system. LTMR receptive field size and organization is also an important factor in determining the firing properties of individual neurons. Single neuron recordings from LTMRs have demonstrated significant sensory specialization across subtypes. The Aβ RA-LTMRs and C-LTMRs both fire action potentials in response to generalized skin indentation and skin stroking in the direction of hair growth (head to tail), differing in their specific response properties [13]. Aδ-LTMRs also fire action potentials in response to skin indentation, but selectively fire in response to skin stroking opposite the direction of hair growth (tail to head) due to their hemicircular arrangement on the caudal side of the hair follicle [16]. Aβ RA-LTMRs, Aδ-LTMRs, and C-LTMRs can all fire action potentials through the stimulation of a single hair follicle. In contrast, the Aβ Field-LTMRs, which have significantly larger receptive fields than other LTMR subtypes, can only fire action potentials through summation when multiple hairs are stimulated simultaneously [17]. These unique properties result in a sensory

system able to accurately localize higher magnitude stimuli through small receptive fields, while also detecting stimuli too faint to trigger action potentials through a single LLE.

The final factor potentially involved in LTMR tiling is an inherent characteristic of the LTMR receptive fields themselves. In adult mice, LTMR axons branch and form highly stereotyped receptive fields, with some subtypes such as the C-LTMRs forming fields innervating on average 15 hair follicles, while on the other extreme the Aβ Field-LTMRs can innervate over 150 hair follicles [17]. Work examining the tiling of LTMR receptive fields has shown an interesting correlation between the number of hair follicles each individual receptive field innervates and the degree of overlap between neighboring homotypic receptive fields. Aβ Field-LTMRs, which have the largest receptive fields, show the least degree of overlap with homotypic neurons. C-LTMRs, which have the smallest receptive fields, show the highest degree of overlap [18].

The ordered development of follicle innervation and interactions between neighboring homotypic neurons during receptive field development raises the question of whether similar mechanisms regulate the organization of central DRG afferents in the spinal cord dorsal horn. The different LTMR subtypes target their axons to specific lamina in the dorsal spinal cord, somatotopically arrange their axons, and show a high degree of synaptic partner specificity [13, 70, 71]. The cellular and molecular mechanisms that govern central afferent organization remain largely unknown, but recent advancements in imaging and genetic tools may open this field to further investigation.

Methods

Mouse husbandry

Mice (*Mus musculus*) were housed in standard conditions, cared for by the Department of Comparative Medicine at Oregon Health and Science University. All animal experimental procedures were approved by OHSU Institutional Animal Care and Use Committee (Protocol # IS00000539) and adhered to the NIH *Guide for the care and use of laboratory animals*. Mice were maintained on a 12-h light/dark cycle and were provided food and water ad libitum. For embryonic tamoxifen administration, the morning of vaginal plug observation was designated as E0.5. Mice were maintained on a mixed genetic background due to experiments being conducted with compound transgenic lines. Mice of both sexes were used, and littermates were used as controls.

Due to the estrogen inhibiting effects of tamoxifen during pregnancy, many female mice fail to initiate labor at the proper time resulting in fetal demise. For all female animals given tamoxifen during pregnancy, pups were delivered by cesarian section at embryonic day 19.5 after mild isoflurane-induced anesthesia and rapid cervical dislocation. After removal from the uterus and amniotic sac, pups were dried gently with a paper towel and warmed on a heating pad at 37 C. Viable pups breathe spontaneously within 1–2 min of removal from the amniotic sac and respond to gentle tactile stimuli within 2–3 min, becoming pink and actively moving within 5–10 min. Viable pups were placed with the litter of a nursing female mouse approximately 15 min after delivery and an equal number of pups were removed from the foster dam's litter. The day of birth or cross-fostering of animals was designated as P0.

Mouse lines

Mouse lines used in this study have all been previously described (Table 1).

Tamoxifen administration

Tamoxifen stock was made by dissolving tamoxifen powder in freshly opened 100% ethanol at a concentration of 150 mg/mL and stored at -80 C until needed. For tamoxifen administration to pregnant female mice, progesterone and β-estradiol were co-administered at a

Table 1 Mouse lines used

Common name	Strain name	Reference	Jax/MGI Reference number
TH^{CreER}	B6;129-*Th*$^{tm1(cre/Esr1)Nat}$/J	[48]	JAX: 008532
$TrkB^{CreERT2}$	B6.129S6(Cg)-*Ntrk2*$^{tm3.1(cre/ERT2)Ddg}$/J	[16]	JAX: 027214
$Ret^{CreERT2}$	$Ret^{tm2(cre/ERT2)Ddg}$	[14]	MGI: 4437245
$Vglut3^{iCre}$	Tg(Slc17a8-icre)1Edw/SealJ	[72]	JAX: 018147
Bax KO	B6.129X1-*Bax*^{tm1Sjk}/J	[46]	JAX: 002994
Ai140D	B6.Cg-$^{Igs7tm140.1(tetO-EGFP,CAG-tTA2)Hze}$/J	[41]	JAX: 030220
R26-iAP	B6;129-Gt(ROSA)26Sor^{tm2Nat}/J	[38]	JAX: 009253

ratio of 1000:500:1, Tamoxifen:progesterone: β-estradiol. Administration timing and dosage are given in associated figure legends. For all administration methods and times, the Tamoxifen/ethanol stock solution was dissolved in sunflower seed oil by vortexing until an emulsion formed. The oil/ethanol mixture was then centrifuged in a heated vacuum centrifuge (SpeedVac) for 15 min to evaporate residual ethanol. Pregnant female mice were administered tamoxifen through oral gavage of 100 µL of sunflower seed oil with dissolved tamoxifen-progesterone-β-estradiol mixture. P12-16 pups were administered tamoxifen through oral gavage of 50 µL of sunflower seed oil with dissolved tamoxifen. P0-P11 pups were administered tamoxifen through IP injection of 10 µL of sunflower seed oil with dissolved tamoxifen.

Tamoxifen doses and timepoints for each use case can be found in Table 2.

Tissue dissection and fixation

See [40] for a detailed description of histology methods. Briefly, animals were euthanized in accordance with IACUC approved protocols. Animals P6 and older were depilated using a commercial depilatory cream (Nair) and were washed with gentle soap and room temperature water. Skin was dissected away from the animal and placed onto a filter paper lined silicone-bottomed dish with a cover. Large fat deposits were trimmed away from the subcutaneous tissue using small scissors and the skin was pinned to the plate, subcutaneous side up, using fine insect pins. Skin was fixed 6 h to overnight at 4 C in 4% paraformaldehyde with gentle agitation. After fixation, skin was washed with PBS for 30 min at room temperature with agitation before progressing to preparation for specific analysis methods. After washing the subcutaneous side of the fixed skin was scraped with a razor blade to remove remaining subcutaneous fat and muscle.

Spinal columns were dissected out and fixed overnight in 4% paraformaldehyde at 4 C with agitation. After fixation spinal columns were washed in PBS for 30 min at room temperature. Spinal columns were incubated overnight in 10% w/v EDTA/10% v/v glycerol in PBS to de-calcify the bones for sectioning through the spinal column (DRG section immunofluorescence and AP staining). Spinal columns were washed 4–5 h in PBS at 4 C to remove EDTA and glycerol before further processing.

Whole mount skin immunofluorescence

Fixed skin prepared as above was washed for 8 h at room temperature in 0.2% v/v Triton X-100 in PBS with gentle agitation, changing the detergent every hour for the first 4 h, then twice more. Skin was moved to blocking solution (5% v/v Normal Donkey Serum, 5% v/v DMSO, 0.25% v/v Triton X-100 in PBS) overnight at 4 C with gentle agitation. Skin was incubated in primary antibodies in blocking solution at the dilutions listed in Table 3 for 5 days at 4 C with gentle agitation. Skin was washed 2 h with 0.2% v/v Triton X-100 in PBS, then 3 h in PBS changing the PBS every hour at room temperature with agitation. Skin was moved to secondary antibodies in blocking solution at a 1:500 concentration for 2–3 days at 4 C with gentle agitation. Skin was washed 1 h in 0.2% v/v Triton X-100, then 2–3 h in PBS at room temperature before dehydration in a methanol gradient (30 min—50% MeOH in PBS, 2 h – 80% MeOH in PBS, overnight – 100% MeOH). After dehydration, skin was cleared in BABB and imaged.

Whole mount skin oil red o staining and imaging

Fixed and washed skin samples were incubated in 60% v/v isopropanol in water for 10 min at room temperature with agitation. Skin was then stained in 0.3% Oil Red O (ORO) in 60% isopropanol at room temperature until dark red staining of sebaceous glands occurred (30 min to 3 h). Skin was then washed twice with 60% isopropanol for 10 min each, then moved to water to store until imaging.

ORO stained skin was imaged by mounting epidermis side up on a glass slide with water and a standard coverslip. A 2 cm^2 area of skin was imaged using a 5 × objective and the number of hair follicles were counted in 10 randomly selected 1 mm^2 fields. The counted field values were averaged together to generate an animal follicle density value.

Table 2 Tamoxifen administration doses and routes

Experiment	Labeling Density	Associated Figure	Mouse Line	Tamoxifen Dose	Admin. Route	Admin. Age
Aδ-LTMR labeling in sections	High	Fig. S2	$TrkB^{CreERT2}$;$R26^{iAP}$	2 doses of 2 mg	P.O. (Maternal)	E12.5, E13.5
Aδ-LTMR fluorescent sparse labeling	Low	Figure 4	$TrkB^{CreERT2}$;Ai140D	0.75 mg	P.O. (Maternal)	E13.5
Aδ-LTMR Cell Body Labeling	High	Figure 5 B, E, F	$TrkB^{CreERT2}$;$R26^{iAP}$	3 doses of 0.5 mg	I.P	P6, P7, P8
Aδ-LTMR RF sparse labeling	Low	Figure 6 A-D	$TrkB^{CreERT2}$; $R26^{iAP}$	0.5 mg	P.O. (Maternal)	E13.5
C-LTMR RF sparse labeling	Low	Figure 6 E–H	TH^{CreER}; $R26^{iAP}$	2 doses of 2 mg	P.O	P14, P15

Table 3 Antibodies used

Antibody	Supplier	Item Number	RRID	Use concentration
Rb α-Calbindin	Swant	CB 38	AB_10000340	1:1000
Rb α-TH	Millipore	AB152	AB_390204	1:1000
Sh α-TH	Millipore	AB1542	AB_90755	1:500
Ms α-Isl1/2	DSHB	39.4D5	AB_2314683	1:250
Gt α-TdTomato	Biorbyt	orb182397	AB_2687917	1:1000
Ck α-GFP	Abcam	ab13970	AB_300798	1:1000
Dk α-Rb IgG 488	ThermoFisher	A-21206		1:500
Dk α-Rb IgG 546	ThermoFisher	A10040		1:500
Dk α-Rb IgG 647	ThermoFisher	A-31573		1:500
Dk α-Ms IgG 647	ThermoFisher	A-31571		1:500
Dk α-Ck IgY 488	Jackson Immuno Research	NC0215979		1:500
Dk α-Ck IgY Cy3	Millipore Sigma	AP194C		1:500
Dk α-Sh 488	ThermoFisher	A-11015		1:500
Dk α-Gt 546	ThermoFisher	A-11056		1:500

Whole mount skin alkaline phosphatase staining

Fixed, washed, and scraped skin was heat treated in 1 mM $MgCl_2$ in PBS at 70 C for 90 min with agitation every 15 min. Skin was allowed to cool to room temperature, then moved to a tube containing 0.1 M Tris/50 mM $MgCl_2$/0.1 M NaCl in water, pH 9.5 with 16.6 µg/mL BCIP and 33.3 µg/mL NBT and 12.5 mM Levamisole for the AP reaction. The AP staining was allowed to develop at room temperature with agitation until labeled neurons were clearly visible in the skin. Fresh buffer and substrate were added after 24 h if staining wasn't satisfactory. After staining progressed to a satisfactory level, skin was pinned to silicone-bottomed dishes with insect pins and dehydrated for 30 min in 50% methanol in water, then 2 h in 80% methanol in water, then overnight at room temperature in 100% methanol. Skin samples were cleared in a 2:1 mixture of Benzyl Benzoate:Benzyl Alcohol (BABB) for 15 min or until optically clear before mounting on a slide in BABB with a standard coverslip for imaging.

Whole mount skin imaging and receptive field quantification

Receptive fields in cleared AP-stained skin were imaged using a Zeiss AxioZoom V.16 Macroscope. The number of LLEs per receptive field were manually counted using the Cell Counter plugin in FIJI/ImageJ. Receptive fields in representative images were semi-manually traced using the Simple Neurite Tracer plugin in Fiji/ImageJ [50]. Receptive fields in cleared immunohistochemically labeled skin were imaged on a Zeiss AxioImager M.2 microscope with an Apotome.2 structured illumination module. The number of LLEs and non-LLE terminal branches were counted manually using the Cell Counter plugin in FIJI/ImageJ.

Skin section cryosection preparation

A 1 cm × 1 cm square of back skin from the anterior midline was taken from fixed mouse skin. The small portion was cryoprotected in a sucrose gradient, 30 min in 10% sucrose in PBS, 2 h in 15% sucrose in PBS, overnight at 4 C in 20% sucrose in PBS. Samples were mounted in OCT media and oriented with the sagittal plane as the cutting face. Samples were rapidly frozen in methylbutane chilled on dry ice. 50 µm sagittal sections were cut, every fifth section mounted on a slide, and allowed to dry at room temperature 2–3 h before moving to a freezer or processing for immunohistochemistry or AP staining as described below.

Spinal cord/DRG section preparation

The T5-T7 segment was dissected from fixed and decalcified spinal columns by cutting through the intervertebral disks between T4/5 and T7/8 with a sharp scalpel blade. The T5-T7 spinal column segment was cryoprotected with a sucrose/OCT gradient, 10% sucrose in PBS for 30 min, 15% sucrose in PBS for 1 h, 20% sucrose in PBS for 2 h, 30% sucrose on PBS for 2 h, half 30% sucrose/half OCT overnight at 4 C with gentle agitation. Samples were mounted in OCT and rapidly frozen in methylbutane cooled on dry ice. 20 µm sections were cut and mounted on slides, collecting every third section, and allowed to dry for 2 h at room temperature before freezing or processing for AP staining then immunohistochemistry as described below.

Section alkaline phosphatase staining

Slide mounted cryosections were washed 3 times for 10 min in PBS at room temperature, then were incubated for 30 min in 1 mM $MgCl_2$ at 70 C. Sections were moved to a humidified slide staining chamber and were stained with 0.1 M Tris/50 mM $MgCl_2$/0.1 M NaCl in water, pH 9.5 with 16.6 µg/mL BCIP and 33.3 µg/mL NBT and 1.25 mM Levamisole until sufficient staining had developed, 4–48 h. Once sufficient staining had developed sections were incubated for 15 min in 1.25 mM levamisole, 0.25 M EDTA in PBS to stop the AP reaction. Sections were then coverslipped with Fluoromount-G or were processed for fluorescence immunohistochemistry.

Section immunohistochemistry

Slide mounted cryosections were washed 3 times for 10 min in PBS at room temperature, then were incubated for 30 min in blocking solution (5% v/v Normal Donkey Serum, 5% v/v DMSO, 0.25% v/v Triton X-100 in PBS). Slides were incubated in primary antibodies diluted in blocking solution at the concentrations listed in Table 3 overnight at 4 C in a humidified staining box. Slides were washed 3 times for 10 min each with PBS, then incubated for 4 h at room temperature in secondary antibodies diluted at 1:500 in blocking solution. Slides were washed 3 times for 10 min each in PBS, adding 1:5000 Hoescht to the first wash. Slides were coverslipped with Fluoromount-G and imaged.

Skin section image quantification

Immunohistochemically labeled and AP-stained skin sections were imaged on a Zeiss AxioImager M.2 microscope with an Apotome.2 structured illumination module. For each animal, a tiled image field approximately 4500 µm wide was captured on a series of 5 nonconsecutive skin sections. The number of hair follicle structures in each section was counted using the DAPI channel. The number of hair follicles with a marker-positive LLE was counted using either the IHC labels described in the text, or AP staining. The proportion of innervated follicles and follicle density measurements from each section were averaged together to generate an average follicle density and follicle innervation proportion value for each animal.

DRG section image quantification

AP stained and immunohistochemically labeled DRG sections were imaged on a Zeiss AxioImager M.2 microscope with an Apotome.2 structured illumination module. Cell counting was performed manually using the Cell Counter plugin in FIJI/ImageJ. To minimize the effect of inter-litter variability in tamoxifen dosing, the number of marker positive cells in *Bax* knockout animals was normalized to the average number of marker positive cells counted in *Bax* heterozygous littermates. The total number of marker positive cells from *Bax* wild type and heterozygous animals were also compared to ensure no effect from single allele loss of *Bax*.

Statistical analysis

All statistics were performed in R v4.1.1 and Microsoft Excel. Statistical tests, *N* values, and *P*-values are described in the text/figure legends where relevant.

Supplementary Information

The online version contains supplementary material available at https://doi.org/10.1186/s13064-023-00170-2.

Additional file 1: Supplemental Figure 1. Hair follicle density decreases relative to body length as mice grow. A) Average body length (nose to base of tail) of an age-matched cohort of 10 wild-type mice in centimeters. Bars represent mean ± s.e.m. One-way ANOVA with Tukey's HSD post-hoc testing (ANOVA $P \leq 0.001$, P1-P3: $P \leq 0.001$, P3-P6: $P \leq 0.001$, P6-P14: $P \leq 0.001$, P14-P21: $P \leq 0.001$. B) Quantification of mouse hair follicle density from Figure 1H normalized to the mean body length of a cohort of 10 same-age mice shown in (A). Bars represent mean ± s.e.m. One-way ANOVA with Tukey's HSD post-hoc testing (ANOVA $P \leq 0.001$, P6-P14 $P \leq 0.001$) $N = 6$(P1), 3(P3), 6(P6), 10(P14), 3(P21), 5(P60).

Additional file 2: Supplemental Figure 2. Aδ-LTMR neurons fully innervate hair follicles by P14. A-C) Representative image of sagittal plane skin sections from a P14 mouse labeled with markers for all neurons (β-III Tubulin, A), Aδ-LTMRs (*TrkB*^{CreERT2};*iAP*), B), and merged channels (C). Insets – Higher magnification images of a β-III Tubulin$^+$/TrkB$^{CreERT2+}$ double positive longitudinal lanceolate ending. 92.2% ± 3% of follicles were innervated by a β-III Tubulin$^+$/TrkB$^+$ LLE. This is similar to previously reported values. $N = 4$ animals. Scale bar – 100 µm, 50 µm inset.

Additional file 3: Supplemental Figure 3. Mice with heterozygous *Bax* deletion have no significant change in the number of neuronal nuclei, Aδ-LTMRs or C-LTMRs compared to wild-type mice. A) Comparison of Islet 1/2$^+$ nuclei in *Bax* wild-type and heterozygous mice shows no significant difference. Bars represent mean ± s.e.m. $N = 7$(WT), 9(Het). Wilcoxon rank sum $P \geq 0.05$. B) Comparison of TrkB$^{CreERT2+}$ cell bodies in *Bax* wild-type and heterozygous mice shows no significant difference. Bars represent mean ± s.e.m. $N = 4$(WT), 7(Het). Wilcoxon rank sum $P \geq 0.05$. C) Comparison of TH$^+$ cell bodies in *Bax* wild-type and heterozygous mice shows no significant difference. Bars represent mean ± s.e.m. $N = 5$(WT), 9(Het). Wilcoxon rank sum $P \geq 0.05$.

Additional file 4: Supplemental Figure 4. *Bax* deficiency does not change hair follicle density. A-C) Representative images of P21 mouse back skin from *Bax* wild-type (A), heterozygous (B), and knockout (C) animals stained with the lipophilic marker Oil Red O to identify hair follicles. Scale bar – 500 µm. D) Quantification of the numbers of hair follicles per square millimeter of back skin. Wild-type: 113.2 ± 3.2 s.e.m. follicles/mm^2, Heterozygous: 104.3 ± 3 s.e.m. follicles/mm^2, Knockout: 102.5 ± 4.1 s.e.m. follicles/mm^2. $N = 4$(WT), 7(Het), 9(KO). One-way ANOVA P= 0.22.

Additional file 5: Supplemental Figure 5. Lack of inter-animal variation in follicles innervated per receptive field between same-genotype animals. A) Quantification of innervated hair follicles per Aδ-LTMR receptive field separated by animal. Each dot represents one quantified receptive field. No significant differences in number of innervated follicles per receptive field were seen between animals within genotype groups. Statistical analysis – One-way ANOVA Bax WT: P= 0.52, Bax Het: P= 0.49, Bax KO: P= 0.86. B) Quantification of innervated hair follicles per C-LTMR receptive field separated by animal. Each dot represents one quantified receptive field. No significant differences in number of innervated follicles per receptive field were seen between animals within genotype groups.

Statistical analysis – One-way ANOVA Bax WT: P= 0.38, Bax Het: P= 0.70, Bax KO: P= 0.72.

Additional file 6: Supplementary Table 1. Summary follicle innervation data shown in Figures 1, 2 and 3. **Supplementary Table 2.** Summary Aδ-LTMR receptive field development data shown in Figure 4. **Supplementary Table 3.** Summary of Bax knockout DRG cell count data shown in Figure 5 and **Supplementary Figure 3.**

Acknowledgements
We thank the Ginty, Badea, and Nathans Labs for the mouse lines used in the preparation of this manuscript. We would also like to thank the members of the Lumpkin Lab for their help with refining the whole-mount skin immunohistochemistry protocol. Finally, we would like to thank the members of the Wright Lab, Murthy Lab, and Kerstein lab for their feedback on the experiments presented in this manuscript.

Authors' contributions
M.B.P was involved in the conceptualization of the project, conducted all experiments, analyzed data, prepared figures, and drafting/editing the manuscript. K.M.W. was involved in the conceptualization of the project, drafting/editing the manuscript, and obtained funding. The author(s) read and approved the final manuscript.

Funding
This work was supported by the National Institutes of Health [R01NS091027 to K.M.W., T32GM071338 to M.B.P.] and a Whitehall Foundation Research Grant [to K.M.W.].

Availability of data and materials
All data used in the preparation of this manuscript will be made available upon request.

Declarations

Ethics approval and consent to participate
All animal experimental procedures were approved and conducted in accordance with the OHSU Institutional Animal Care and Use Committee (Protocol # IS00000539) and adhered to the NIH ***Guide for the care and use of laboratory animals***.

Consent for publication
Not applicable.

Competing interests
The authors declare no competing interests.

Received: 23 September 2022 Accepted: 20 April 2023
Published online: 27 April 2023

References

1. Rice FL, Albrecht PJ. Cutaneous Mechanisms of Tactile Perception: Morphological and Chemical Organization of the Innervation to the Skin. The Senses: A Comprehensive Reference. 2008;6:1–31.
2. Cain DM, Khasabov SG, Simone DA. Response properties of mechanoreceptors and nociceptors in mouse glabrous skin: An in vivo study. J Neurophysiol. 2001;85:1561–74.
3. Burgess PR, Petit D, Warren RM. Receptor types in cat hairy skin supplied by myelinated fibers. J Neurophysiol. 1968;31:833–48.
4. Paré M, Smith AM, Rice FL. Distribution and terminal arborizations of cutaneous mechanoreceptors in the glabrous finger pads of the monkey. J Comp Neurol. 2002;445:347–59.
5. Knibestöl M. Stimulus—response functions of rapidly adapting mechanoreceptors in the human glabrous skin area. J Physiol. 1973;232:427–52.
6. Leem JW, Willis WD, Chung JM. Cutaneous sensory receptors in the rat foot. J Neurophysiol. 1993;69:1684–99.
7. Halata Z. Sensory innervation of the hairy skin (light-and electronmicroscopic study). J Invest Dermatol. 1993;1 Suppl(12):75S-81S.
8. Iggo A, Muir AR. The structure and function of a slowly adapting touch corpuscle in hairy skin. J Physiol. 1969;200:763–96 Available from: http://www.ncbi.nlm.nih.gov/pubmed/4974746.
9. Lynn B, Carpenter SE. Primary afferent units from the hairy skin of the rat hind limb. Brain Res. 1982;238:29–43 Available from: http://www.jstor.org/stable/10.2307/j.ctv1z7kkb3.7University of Iowa Press.
10. Brown AG, Iggo A. A quantitative study of cutaneous receptors and afferent fibres in the cat and rabbit. J Physiol. 1967;193:707–33 Available from: https://onlinelibrary.wiley.com/doi/10.1113/jphysiol.1967.sp008390.
11. Lewin GR, McMahon SB. Physiological properties of primary sensory neurons appropriately and inappropriately innervating skin in the adult rat. J Neurophysiol. 1991;66:1205–17.
12. Horch KW, Tuckett RP, Burgess PR. A key to the classification of cutaneous mechanoreceptors. J Invest Dermatol. 1977;69:75–82 Available from: http://www.ncbi.nlm.nih.gov/pubmed/874346Elsevier Inc.
13. Li L, Rutlin M, Abraira VE, Cassidy C, Kus L, Gong S, et al. The Functional Organization of Cutaneous Low-Threshold Mechanosensory Neurons. Cell. 2011;147:1615–27 (http://dx.doi.org/10.1016/j.cell.2011.11.027).
14. Luo W, Enomoto H, Rice FL, Milbrandt J, Ginty DD. Molecular Identification of Rapidly Adapting Mechanoreceptors and Their Developmental Dependence on Ret Signaling. Neuron. 2009;64:841–56 Available from: http://linkinghub.elsevier.com/retrieve/pii/S089662730900885XElsevier Inc.
15. Wu H, Williams J, Nathans J. Morphologic diversity of cutaneous sensory afferents revealed by genetically directed sparse labeling. Elife. 2012;1:1–20 Available from: http://elifesciences.org/lookup/doi/10.7554/eLife.00181.
16. Rutlin M, Ho CY, Abraira VE, Cassidy C, Bai L, Woodbury CJ, et al. The Cellular and Molecular Basis of Direction Selectivity of Aδ-LTMRs. Cell. 2014;159:1640–51 Available from: http://linkinghub.elsevier.com/retrieve/pii/S0092867414015153Elsevier Inc.
17. Bai L, Lehnert BP, Liu J, Neubarth NL, Dickendesher TL, Nwe PH, et al. Genetic Identification of an Expansive Mechanoreceptor Sensitive to Skin Stroking. Cell. 2015;163:1783–95 Available from:http://linkinghub.elsevier.com/retrieve/pii/S0092867415016220Elsevier Inc.
18. Kuehn ED, Meltzer S, Abraira VE, Ho C-Y, Ginty DD. Tiling and somatotopic alignment of mammalian low-threshold mechanoreceptors. Proceedings of the National Academy of Sciences. 2019;201901378. Available from: http://www.pnas.org/lookup/doi/10.1073/pnas.1901378116/10.1073/pnas.1901378116.
19. Li L, Ginty DD. The structure and organization of lanceolate mechanosensory complexes at mouse hair follicles. Elife. 2014;3:e01901.
20. Grueber WB, Jan LY, Jan YN. Tiling of the Drosophila epidermis by multidendritic sensory neurons. Development. 2002;129:2867–78 Available from: http://dev.biologists.org/content/129/12/2867abstract.
21. Grueber WB, Ye B, Moore AW, Jan LY, Jan YN. Dendrites of Distinct Classes of Drosophila Sensory Neurons Show Different Capacities for Homotypic Repulsion. Current Biology. 2003;13:618–26 Available from: http://linkinghub.elsevier.com/retrieve/pii/S0960982203002070.
22. Grueber WB, Graubard K, Truman JW. Tiling of the body wall by multidendritic sensory neurons in Manduca sexta. J Comp Neurol. 2001;440:271–83.
23. Blackshaw SE, Nicholls JG, Parnas I. Expanded receptive fields of cutaneous mechanoreceptor cells after single neurone deletion in leech central nervous system. J Physiol. 1982;326:261–8 Available from: http://www.ncbi.nlm.nih.gov/pubmed/7108791.
24. Kramer AP, Kuwada JY. Formation of the receptive fields of leech mechanosensory neurons during embryonic development. J Neurosci Soc Neurosci. 1983;3:2474–86.
25. Sagasti A, Guido MR, Raible DW, Schier AF. Repulsive Interactions Shape the Morphologies and Functional Arrangement of Zebrafish Peripheral Sensory Arbors. Current Biology. 2005;15:804–14 Available from: http://linkinghub.elsevier.com/retrieve/pii/S0960982205003428.
26. Reese BE, Raven MA, Stagg SB. Afferents and homotypic neighbors regulate horizontal cell morphology, connectivity, and retinal coverage. J Neurosci. 2005;25:2167–75.
27. Huckfeldt RM, Schubert T, Morgan JL, Godinho L, di Cristo G, Huang ZJ, et al. Transient neurites of retinal horizontal cells exhibit columnar tiling via homotypic interactions. Nat Neurosci. 2009;12:35–43.

28. Keeley PW, Lebo MC, Vieler JD, Kim JJ, st. John AJ, Reese BE. Interrelationships between Cellular Density, Mosaic Patterning, and Dendritic Coverage of VGluT3 Amacrine Cells. The Journal of Neuroscience [Internet]. 2020;JN-RM-1027-20. Available from: http://www.jneurosci.org/lookup/doi/10.1523/JNEUROSCI.1027-20.2020.
29. Lee SCS, Cowgill EJ, Al-Nabulsi A, Quinn EJ, Evans SM, Reese BE. Homotypic Regulation of Neuronal Morphology and Connectivity in the Mouse Retina. J Neurosci. 2011;31:14126–33 Available from: http://www.jneurosci.org/cgi/doi/10.1523/JNEUROSCI.2844-11.2011.
30. Farajian R, Raven MA, Cusato K, Reese BE. Cellular positioning and dendritic field size of cholinergic amacrine cells are impervious to early ablation of neighboring cells in the mouse retina. Vis Neurosci. 2004;21:13–22 (Oregon Health & Science University).
31. Paus R, Müller-Röver S, van der Veen C, Maurer M, Eichmüller S, Ling G, et al. A comprehensive guide for the recognition and classification of distinct stages of hair follicle morphogenesis. J Investig Dermatol. 1999;113:523–32.
32. Müller-Röver S, Handjiski B, van der Veen C, Eichmüller S, Foitzik K, McKay IA, et al. A comprehensive guide for the accurate classification of murine hair follicles in distinct hair cycle stages. J Investig Dermatol. 2001;117:3–15.
33. Peters EMJ, Botchkarev VA, Müller-Röver S, Moll I, Rice FL, Paus R. Developmental timing of hair follicle and dorsal skin innervation in mice. J Comp Neurol. 2002;448:28–52. Available from: http://doi.wiley.com/10.1002/cne.10211.
34. Meltzer S, Boulanger K, Osei-Asante E, Handler A, Zhang Q, Sano C, et al. A role for axon-glial interactions and Netrin-G1 signaling in the formation of low-threshold mechanoreceptor end organs. Proceedings of the National Academy of Sciences. 2022;119(43) https://doi.org/10.1073/pnas.2210421119.
35. Usoskin D, Furlan A, Islam S, Abdo H, Lönnerberg P, Lou D, et al. Unbiased classification of sensory neuron types by large-scale single-cell RNA sequencing. Nat Neurosci. 2014;18:145–53 Available from: http://www.nature.com/doifinder/10.1038/nn.3881Nature Publishing Group.
36. Lou S, Duan B, Vong L, Lowell BB, Ma Q. Runx1 Controls Terminal Morphology and Mechanosensitivity of VGLUT3-expressing C-Mechanoreceptors. J Neurosci. 2013;33:870–82 Available from: http://www.jneurosci.org/cgi/doi/10.1523/JNEUROSCI.3942-12.2013.
37. Seal RP, Wang X, Guan Y, Raja SN, Woodbury CJ, Basbaum AI, et al. Injury-induced mechanical hypersensitivity requires C-low threshold mechanoreceptors. Nature. 2009;462:651–5. https://doi.org/10.1038/nature08505Nature Publishing Group.
38. Badea TC, Wang Y, Nathans J. A noninvasive genetic/pharmacologic strategy for visualizing cell morphology and clonal relationships in the mouse. J Neurosci. 2003;23:2314–22 Available from: http://www.ncbi.nlm.nih.gov/pubmed/12657690.
39. Sharma N, Flaherty K, Lezgiyeva K, Wagner DE, Klein AM, Ginty DD. The emergence of transcriptional identity in somatosensory neurons. Nature. 2020;577:392–8 Available from: http://www.nature.com/articles/s41586-019-1900-1Springer US.
40. Pomaville MB, Wright KM. Immunohistochemical and Genetic Labeling of Hairy and Glabrous Skin Innervation. Curr Protoc. 2021;1:1–31.
41. Daigle TL, Madisen L, Hage TA, Valley MT, Knoblich U, Larsen RS, et al. A Suite of Transgenic Driver and Reporter Mouse Lines with Enhanced Brain-Cell-Type Targeting and Functionality. Cell Cell Press. 2018;174:465-480.e22.
42. Suzuki H, Aoyama Y, Senzaki K, Vincler M, Wittenauer S, Yoshikawa M, et al. Characterization of sensory neurons in the dorsal root ganglia of Bax-deficient mice. Brain Res. 2010;1362:23–31 Available from: http://linkinghub.elsevier.com/retrieve/pii/S0006899310020068Elsevier B.V.
43. Kinugasa T, Kudo N, Ozaki S. Peripheral targets influence sensory-motor connectivity in the neonatal spinal cord: Sciatic nerve axotomy in Bax-deficient mice. Neurosci Res. 2006;54:30–7.
44. Sun W, Winseck A, Vinsant S, Park OH, Kim H, Oppenheim RW. Programmed cell death of adult-generated hippocampal neurons is mediated by the proapoptotic gene bax. J Neurosci. 2004;24:11205–13.
45. Takahashi Y, Nakajima Y. Dermatomes in the rat limbs as determined by antidromic stimulation of sensory C-fibers in spinal nerves. Pain. 1996;67:197–202.
46. Knudson CM, Tung KSK, Tourtellotte WG, Brown GAJ, Korsmeyer SJ. Bax-deficient mice with lymphoid hyperplasia and male germ cell death. Science (1979). 1979;1995(270):96–9 Available from: http://science.sciencemag.org/content/270/5233/96.abstract.
47. Badea TC, Hua ZL, Smallwood PM, Williams J, Rotolo T, Ye X, et al. New Mouse Lines for the Analysis of Neuronal Morphology Using CreER(T)/loxP-Directed Sparse Labeling. Ikezu T, editor. PLoS One. 2009;4:e7859 Available from: https://dx.plos.org/10.1371/journal.pone.0007859.
48. Rotolo T, Smallwood PM, Williams J, Nathans J. Genetically-Directed, Cell Type-Specific Sparse Labeling for the Analysis of Neuronal Morphology. Ben-Jacob E, editor. PLoS One [Internet]. Public Library of Science; 2008 [cited 2022 Jun 20];3:e4099. Available from: https://dx.plos.org/10.1371/journal.pone.0004099/10.1371/journal.pone.0004099.
49. Schindelin J, Arganda-Carreras I, Frise E, Kaynig V, Longair M, Pietzsch T, et al. Fiji: An open-source platform for biological-image analysis. Nat Methods. Nature Publishing Group; 2012. 676–82.
50. Longair MH, Baker DA, Armstrong JD. Simple Neurite Tracer: open source software for reconstruction, visualization and analysis of neuronal processes. Bioinformatics. 2011;27:2453–4 Available from: https://academic.oup.com/bioinformatics/article-lookup/doi/10.1093/bioinformatics/btr390Oxford Academic [cited 2022 Jun 20].
51. Mann SJ. Prenatal formation of hair follicle types. Anat Rec. 1962;144:135–41. Available from: https://onlinelibrary.wiley.com/doi/10.1002/ar.1091440208[cited 2022 Jul 29].
52. Hardy MH. The development of mouse hair in vitro with some observations on pigmentation. J Anat. 1949;83:364–84, 3 pl Available from: http://www.ncbi.nlm.nih.gov/pubmed/15394398.
53. Landy MA, Goyal M, Lai HC. Nociceptor subtypes are born continuously over DRG development. Dev Biol. 2021;479:91–8 https://doi.org/10.1016/j.ydbio.2021.07.018Elsevier Ltd.
54. Bate CM. Pioneer neurones in an insect embryo. Nature Nature. 1976;260:54–6.
55. Edwards JS. Pathfinding by Arthropod Sensory Nerves. Identified Neurons and Behavior of Arthropods. Boston: Springer; 1977. p. 483–93.
56. Keshishian H. The origin and morphogenesis of pioneer neurons in the grasshopper metathoracic leg. Dev Biol Dev Biol. 1980;80:388–97.
57. Edwards JS, Chen SW, Berns MW. Cercal sensory development following laser microlesions of embryonic apical cells in Acheta domesticus. J Neurosci Neurosci. 1981;1:250–8.
58. Klose M, Bentley D. Transient pioneer neurons are essential for formation of an embryonic peripheral nerve. Science (1979). 1989;245:982–4.
59. Pittman AJ, Law MY, Chien CB. Pathfinding in a large vertebrate axon tract: Isotypic interactions guide retinotectal axons at multiple choice points. Development. 2008;135:2865–71.
60. Melançon E, Liu DWC, Westerfield M, Eisen JS. Pathfinding by identified zebrafish motoneurons in the absence of muscle pioneers. J Neurosci Soci Neurosci. 1997;17:7796–804.
61. Pike SH, Melancon EF, Eisen JS. Pathfinding by zebrafish motoneurons in the absence of normal pioneer axons. Development. 1992;114:825–31.
62. Tuttle A, Drerup CM, Marra M, McGraw H, Nechiporuk AV. Retrograde ret signaling controls sensory pioneer axon outgrowth. Elife. eLife Sciences Publications Ltd; 2019;8.
63. Buss RR, Sun W, Oppenheim RW. Adaptive roles of programmed cell death during nervous system development. Annu Rev Neurosci. Annual Reviews; 2006. p. 1–35.
64. Oppenheim RW, Prevette D, Qin-Wei Y, Collins F, MacDonald J. Control of embryonic motoneuron survival in vivo by ciliary neurotrophic factor. Science. 1979;1991(251):1616–8. Available from: https://www.science.org/doi/10.1126/science.2011743.
65. Fariñas I, Jones KR, Backus C, Wang XY, Reichardt LF. Severe sensory and sympathetic deficits in mice lacking neurotrophin-3. Nature. 1994;369:658–61.
66. White FA, Keller-Peck CR, Michael Knudson C, Korsmeyer SJ, Snider WD. Widespread elimination of naturally occurring neuronal death in Bax-deficient mice. J Neurosci Soc Neurosci. 1998;18:1428–39.
67. Patel TD, Jackman A, Rice FL, Kucera J, Snider WD. Development of sensory neurons in the absence of NGF/TrkA signaling in vivo. Neuron Cell Press. 2000;25:345–57.
68. Stantcheva KK, Iovino L, Dhandapani R, Martinez C, Castaldi L, Nocchi L, et al. A subpopulation of itch-sensing neurons marked by Ret and somatostatin expression. EMBO Rep. 2016;17:585–600 Available from: http://embor.embopress.org/lookup/doi/10.15252/embr.201540983.

69. Meltzer S, Boulanger K, Chirila A, Osei-Asante E, DeLisle M, Zhang Q, et al. γ-Protocadherins control synapse formation and peripheral branching of touch sensory neurons. Neuron. Cell Press; 2023 in press. Available from: https://doi.org/10.1016/j.neuron.2023.03.012.
70. Abraira VE, Kuehn ED, Chirila AM, Springel MW, Toliver AA, Zimmerman AL, et al. The Cellular and Synaptic Architecture of the Mechanosensory Dorsal Horn. Cell. 2017;168:295-310.e19. https://doi.org/10.1016/j.cell.2016.12.010. (Elsevier).
71. Odagaki K, Kameda H, Hayashi T, Sakurai M. Mediolateral and dorsoventral projection patterns of cutaneous afferents within transverse planes of the mouse spinal dorsal horn. Journal of Comparative Neurology [Internet]. 2018;1–13. Available from: http://doi.wiley.com/10.1002/cne.24593.
72. Grimes WN, Seal RP, Oesch N, Edwards RH, Diamond JS. Genetic targeting and physiological features of VGLUT3+ amacrine cells. Vis Neurosci. 2011;28:381–92.

Publisher's Note